Applied Catalysis B: Environmental 96 (2010) 18–27

Contents lists available at ScienceDirect

Applied Catalysis B: Environmental

journal homepage: www.elsevier.com/locate/apcatb

Low temperature catalytic steam reforming of ethanol. 1. The effect of the support on the activity and stability of Pt catalysts

P. Ciambelli, V. Palma *, A. Ruggiero

Dipartimento di Ingegneria Chimica e Alimentare, Università degli Studi di Salerno, Via Ponte Don Melillo, 84084 Fisciano, SA, Italy

ARTICLE INFO

Article history:
Received 14 July 2009
Received in revised form 26 January 2010
Accepted 30 January 2010
Available online 6 February 2010

Keywords:
Fuel cell
Hydrogen production
Low temperature ethanol steam reforming
Pt/CeO_2 catalyst
Pt/Al_2O_3 catalyst
Ethanol pre-reforming
Catalyst deactivation

ABSTRACT

The effects of the support (alumina or ceria) on the activity, selectivity and stability of 1 wt% Pt catalyst for the low temperature ethanol steam reforming reaction have been investigated. Experimental results in the range 300–450 °C showed a better performance of ceria supported catalyst, especially with reference to deactivation rate. The characterizations of catalysts reveal the presence of very well dispersed PtO_x in the ceria that, during the calcination step, is stabilized in the highest oxidation state, in contrast with Al_2O_3. Moreover, H_2 TPR, and TPD showed that the better performances of the ceria supported catalyst are strictly linked to the greater ability of CeO_2 to release and store oxygen, resulting in higher stability with respect to alumina supported catalysts. Coke formation, investigated by TPO experiments, occurred on supports and catalysts. However, more stable carbonaceous species were found on Al_2O_3 and Pt/Al_2O_3, likely responsible for the higher deactivation rate with respect to CeO_2 supported Pt catalyst.

Finally, catalytic activity, selectivity and stability of Pt/CeO_2 catalyst increase by increasing the Pt load in the range 1–5 wt%. The best catalyst formulation (5 wt% Pt on CeO_2) was selected for further studies. It is worthwhile that this catalyst is also active for the water gas shift conversion of CO to CO_2, resulting in the absence of CO in the reformate product.

1. Introduction

In the last years hydrogen has attracted significant research interest as an alternative fuel allowing to reduce the consumption of fossil fuels and the co-production of greenhouse gas and air pollutants. To date hydrogen is industrially produced by catalytic steam reforming of fossil fuels, mostly methane [1], but it could be also obtained from renewable energy sources such as bio-ethanol. Therefore, a large number of studies of ethanol conversion by steam reforming (SR) to produce H_2 for polymer electrolyte membrane fuel cells (PEMFC) have been reported [2–4]. PEMFC powered by hydrogen are well-suited for both vehicular and decentralized stationary facilities such as combined heat and power generation for houses and small-scale commercial applications. Since PEMFC require a continuous supply of hydrogen, the use of an in situ catalytic fuel processor allowing the effective conversion into hydrogen is a potentially feasible solution. Ethanol as fuel is widely available, easily transportable, safe to handle and less toxic compared to methanol.

In the case of SR, despite the high hydrogen yield, a critical issue for application is the high reaction temperatures required by thermodynamic constrains, which favor formation of CO, a poison for the anode of the fuel cell. As a consequence, downstream purification processes for further CO conversion such as water gas shift (WGS) and preferential oxidation (PROX) are required, resulting in higher hydrogen cost and larger size and weight of the ethanol processor. Moreover, the high-reforming temperature coupled with the lower temperature of purification steps suffers from thermal inefficiencies.

Thermodynamically, low temperature SR of ethanol depresses CO formation, allowing the overall thermal efficiency be increased and the costs be reduced, but faces the challenge of the favored formation of CH_4 and undesirable reaction by-products leading to coke formation [5–8], causing reduced H_2 selectivity and poor catalyst life. Thus, kinetic rather than thermodynamic control of the reaction is required. Moreover, complete ethanol conversion is essential for the process to be economical.

The state of art of the catalytic SR of ethanol has been recently reviewed [9]. Ethanol conversion by steam reforming includes several reaction steps that require catalytic formulations capable to: (i) dehydrogenate ethanol, (ii) break the carbon–carbon bonds of surface intermediates to produce CO and CH_4 and (iii) water reforming C_1 products to hydrogen. Additionally, candidate catalysts must have high thermal stability, a critical requirement at the high temperature range (823–1073 K) of reforming reactions operation. All the above requirements direct the choice of both

* Corresponding author. Tel.: +39 089964147; fax: +39 089964057.
E-mail address: vpalma@unisa.it (V. Palma).

0926-3373/$ – see front matter © 2010 Elsevier B.V. All rights reserved.
doi:10.1016/j.apcatb.2010.01.029

active phase and support at the right catalyst formulation. The reaction has been investigated on several catalysts based on bulk metal oxides [10,11] and Ni [12,13], Co [14,15], Pd, Pt, Rh [16–18] as active phase supported on various oxides promoted with alkali or alkali-earth compounds to improve both thermal stability and resistance to coke formation.

Among noble metals, thermal, high activity in C–C bond breaking [19] and WGS conversion [20] makes Pt a suitable active phase for ethanol reforming reactions. Moreover, the addition of CeO_2 to platinum has been reported to be effective for both ethanol decomposition [21] and WGS conversion [22]. The promoting effect of CeO_2 has been attributed [23] to: (i) higher reducibility of ceria in the presence of Pt, (ii) higher dispersion of Pt over CeO_2, and (iii) prevention of Pt metal particles sintering. It is also reported that the presence of ceria and ceria-zirconia solid solutions also improves the catalyst resistance to coke deposition due to the oxygen storage-release capability, which facilitates coke gasification [24,25].

The analysis of literature on SR of ethanol shows that the most papers refer to catalytic studies at high temperature (>773 K), while limited attention has been devoted to low temperature conditions. Moreover, many questions concerning catalyst stability, reaction and deactivation mechanism are still open questions [26]. Particularly at low temperature different reaction pathways may be favored depending on the support nature, changing significantly the activity, stability and product distribution of ethanol SR over supported Pt catalysts [27,28].

The objective of the present study was to develop a highly efficient, more stable and cost effective catalyst for SR of ethanol at relatively low temperature to produce H_2 with high selectivity and low CO in the outlet gas, which will make the downstream CO clean-up relatively easier for PEMFC applications. In this first part a series of supported Pt catalysts have been studied. The effects of the support (alumina or ceria) and Pt concentration on the catalyst activity, selectivity and stability have been investigated and the best catalyst formulation with respect to selectivity and stability has been identified.

In the second part [29] preliminary results of a kinetic investigation of SR of ethanol on the selected Pt/CeO_2 catalyst and a proposed reaction mechanism are reported. In the third part, the effect of ethanol concentration on the catalytic performance will be investigated.

2. Experimental

2.1. Catalyst preparation and characterization

Commercially available CeO_2 (Aldrich) and Al_2O_3 (Fisons) with a BET surface area of 80 and 160 m^2/g, respectively, were used as catalyst supports. Pt-containing catalysts were prepared by impregnation with aqueous solution of $PtCl_4$, drying at 120 °C overnight, calcination in air (10 °C/min to 600 °C and staying 3 h at that temperature).

Powder X-ray diffraction (XRD) patterns were recorded with a D-max-RAPID X-ray microdiffractometer (Cu-Kα radiation) operated at 40 kV and 20 mA.

The specific surface area (S_{BET}) of the catalysts was calculated from a multipoint BET analysis of nitrogen adsorption data obtained with Sorptometer 1040 (Costech) instrument.

Temperature programmed reduction (TPR) was carried out before each ethanol steam reforming test: the fresh sample was reduced in situ at 600 °C for 1 h at 20 °C/min heating rate under 1000 (stp)cm^3/min flow rate of a gas mixture containing 5 vol% of H_2 in N_2.

To understand and to explain the different performance of the catalysts and to identify the products, beyond CH_4, CO, CO_2 and H_2, formed during reaction, the surface species adsorbed on the catalyst surface were investigated. For this purpose temperature programmed desorption (TPD) experiments of surface residues formed during the run time were carried out with the following

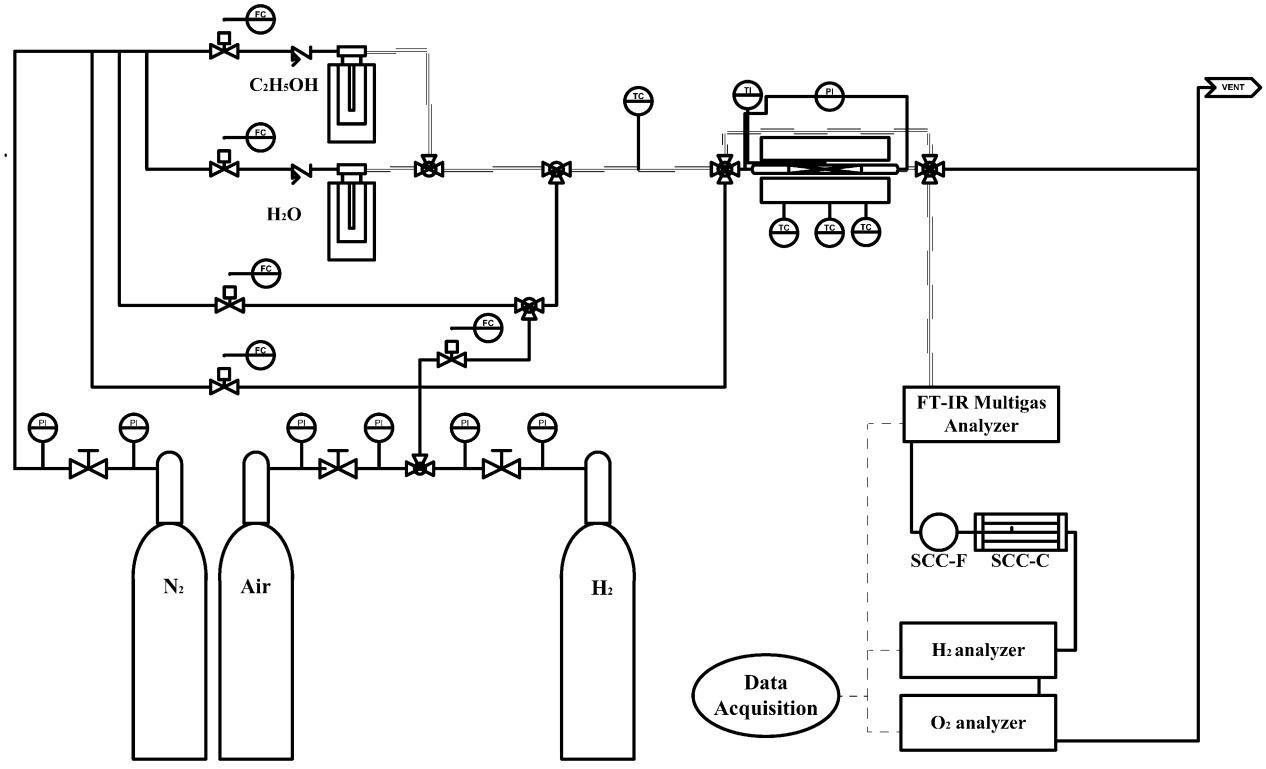

Fig. 1. Laboratory plant for catalytic test of steam reforming of ethanol.

procedure: after catalytic test the reactor was cooled to ~ 100 °C still flowing the reaction stream, then 1000 (stp)cm^3/min of pure N_2 were flowed during hours, before starting a linear temperature ramp at 20 °C/min rate from 100 to 600 °C.

The amount of coke deposited on the surface of catalyst samples recovered after TPD experiments was evaluated by continuously monitoring the concentration of CO and CO_2 evolved during temperature programmed oxidation (TPO) in 1000 (stp)cm^3/min air flow at 20 °C/min from 100 to 600 °C.

2.2. Catalytic activity testing

The laboratory plant for steam reforming catalytic testing is sketched in Fig. 1. Activity tests were carried out with a continuous flow fixed bed reactor (18 mm i.d.) placed in a three zone electric oven, at atmospheric pressure, in the temperature range 300–450 °C. The catalyst (particle size 180–355 μm) was held in place in the reactor by quartz wool. Ethanol and water were fed by saturating a N_2 stream at controlled temperature. The mixture was diluted with a N_2 stream, giving a typical feed gas composition of $C_2H_5OH/H_2O/N_2$ = 0.5/1.5/98 vol%. The gas hourly space velocity was 15,000 h^{-1} and the temperature was 300 °C.

The outlet reactor concentrations of C_2H_5OH, H_2O, CH_4, CO, CO_2 and other by-products were monitored with an on line Nicolet Antaris IGS FT-IR multigas analyzer (Thermo Electron S.p.A.). The spectrophotometer is equipped with a two fixed path length heated gas cell operating at temperatures up to 185 °C coupled with an MCT-A detector cooled with liquid nitrogen. The spectrophotometer is also controlled by a dedicated software able to analyse simultaneously up to 100 different gaseous species. The spectra were collected with a 2-m gas cell, whose temperature was set at 150 °C. Temperature and pressure were monitored and used to correct gas concentrations. The data were acquired at a resolution of 0.5 cm^{-1}. The H_2 concentration in the gas was determined by a thermoconductivity analyzer (ABB, CALDOS 27). This configuration of the FT-IR analyzer allows to work at the highest sensitivity with respect to the secondary compounds, but it limits the maximum ethanol concentration in the feed gas to about 0.5 vol%.

3. Results

3.1. Physical and chemical characterization

The values of specific surface area of both supports and catalysts with 1% nominal Pt content are listed in Table 1. The BET surface area of calcined CeO_2 was 46 m^2/g. Upon 1% platinum loading the specific surface area did not change, while in the case of alumina it increased to 187 m^2/g.

XRD diffraction patterns of supports alone, and 1-Pt loaded samples after calcination are shown in Fig. 2. For both samples, only peaks assigned the supports were found, suggesting that Pt is well dispersed on the support surface.

3.2. Temperature programmed reduction

The 1-Pt/Al_2O_3 sample shows a first peak at 105 °C, a broad composite peak centered at 245 °C, and a small peak centered at 393 °C. In the case of 1-Pt/CeO_2 catalyst the reduction profile is characterized by three distinct peaks, with the first one centered at about 200 °C, followed by two minor peaks centered, respectively, at about 360 and 460 °C (Fig. 3).

The single contributions to the hydrogen uptake, as calculated after peaks deconvolution, are reported in Table 2. These reduction behavior may be explained considering the presence of different PtO_x species with different reducibilities. In particular, the lower temperature peaks can be assigned to the reduction of PtO_2 species [30].

For the higher temperature peak, it must be considered that, particularly for 1-Pt/Al_2O_3, prepared from chloride precursor, platinum could be present also as Pt oxychlorinated species, which are reduced at higher temperature [31]. Anyway, the overall hydrogen uptake is lower than that required for the reduction of PtO_2 species, suggesting that in the 1-Pt/Al_2O_3 sample, even after calcination step, only a small amount of platinum is present at the highest oxidation state. The comparison with results of TPR of 1-Pt/CeO_2 catalyst is dramatic, with a very different H_2 consumption; in

Table 1
Specific surface area (SSA) of Al_2O_3 and CeO_2 and 1-Pt supported catalysts.

Samples	Nominal metal content (wt%)	SSA (m^2/g)
Al_2O_3	–	160
CeO_2	–	46
1-Pt/Al_2O_3	1	187
1-Pt/CeO_2	1	47

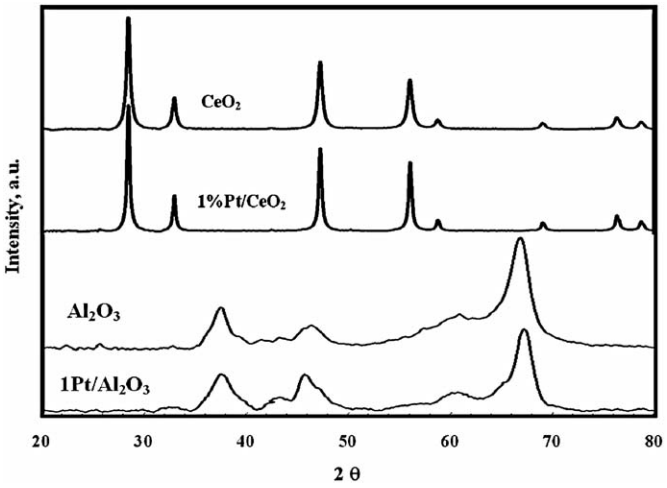

Fig. 2. XRD patterns of calcined CeO_2, Al_2O_3 supports and after 1-Pt load.

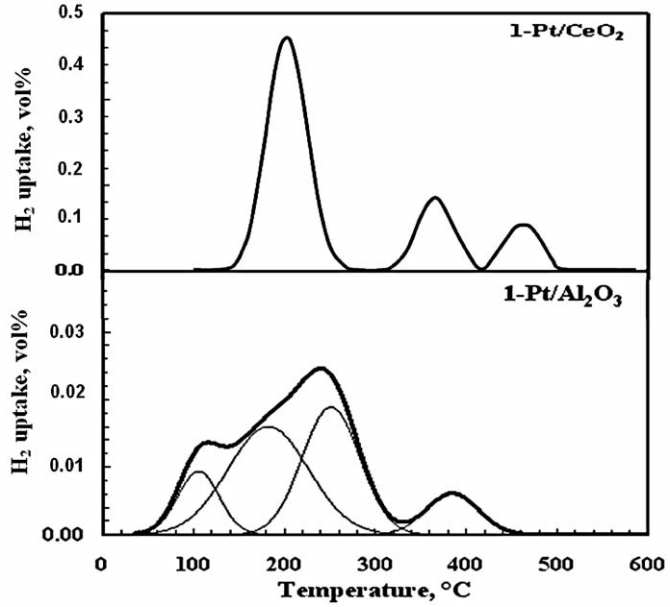

Fig. 3. TPR profiles of 1-Pt/Al_2O_3 and 1-Pt/CeO_2 catalysts.

Table 2
TPR H_2 uptake of 1-Pt/Al_2O_3 and 1-Pt/CeO_2 catalysts.

	T (°C)	H_2 (μmol/g)	H_2 (μmol/g for $Pt^{4+} \rightarrow Pt^0$)
1-Pt/Al_2O_3	105	3.8	103
	182	9.2	
	251	6.4	
	384	2.0	
1-Pt/CeO_2	203	117.4	103
	366	32.8	–
	462	22.8	–

this case it is very close to the amount calculated for the complete Pt(4+) reduction to Pt(0) just by considering only the first peak. For the additional H_2 consumption relevant to the higher temperature peaks, we suggest that it may be assigned to the support reduction, enhanced by the Pt(0) presence. Since pure CeO_2 shows a peak at 480 °C, characteristic of the reduction of capping oxygen anions attached to a surface Ce^{4+} ion [32,33], we conclude that the presence of platinum modifies the features of the ceria reduction and suggest the presence of an H_2 spillover mechanism from Pt surface to CeO_2 surface, enhanced by the high metal dispersion on the support surface. In particular, the profile of 1-Pt/CeO_2 exhibits a single symmetric reduction peak centered at 203 °C, indicating a high dispersion of PtO_x particles with uniform particle size distribution.

Therefore, we can say that for temperature lower than 300 °C the higher temperature reduction peak can be assigned to the presence of highly dispersed PtO_x species on the CeO_2 surface and the presence of direct Pt–O–Ce bonding, where the strong interaction of PtO_x with CeO_2 retards the reduction of the supported PtO_x phase to metallic Pt [34].

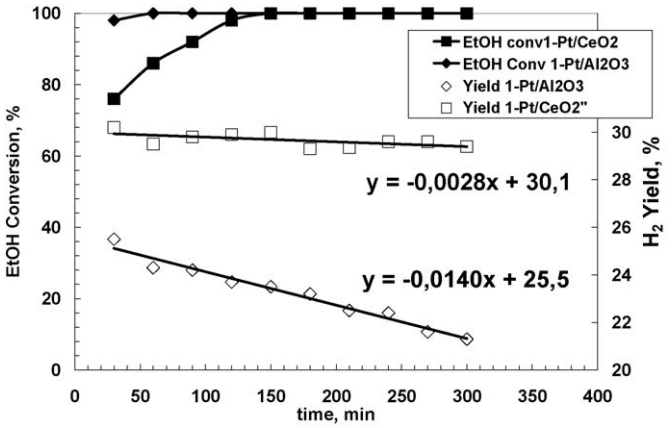

Fig. 4. Ethanol conversion and H_2 yield on 1 wt% Pt catalysts supported on CeO_2 and Al_2O_3 versus time on stream in ethanol steam reforming. *Experimental conditions*: T = 300 °C; C_2H_5OH = 0.5 vol%; C_2H_5OH:H_2O:N_2 = 0.5:1.5:98; Q_{Tot} = 1000 (stp)cm^3/min; GHSV: 15,000 h^{-1}.

3.3. Effect of support on catalytic activity

The role of support in ethanol SR was firstly investigated at constant reaction temperature (300 °C) with CeO_2 and Al_2O_3.

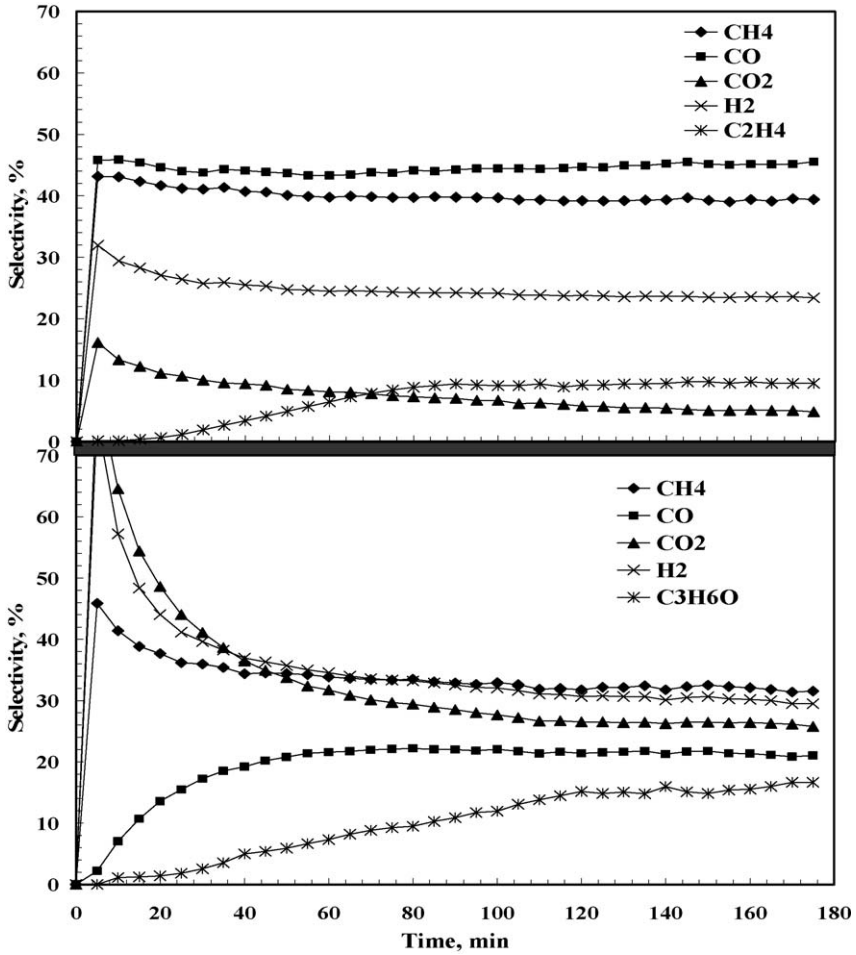

Fig. 5. Products selectivity versus time on stream on 1-Pt/Al_2O_3, and 1-Pt/CeO_2. *Experimental conditions*: T = 300 °C; C_2H_5OH = 0.5 vol%; C_2H_5OH:H_2O:N_2 = 0.5:1.5:98; Q_{Tot} = 1000 (stp)cm^3/min; GHSV: 15,000 h^{-1}.

Table 3
Selectivity to CH_4, CO, CO_2 and H_2 after 3 h of time on stream of Pt catalysts supported on CeO_2 and Al_2O_3 with different metal loadings in ethanol steam reforming. *Experimental conditions*: $T = 300\,^{\circ}C$; $C_2H_5OH = 0.5$ vol%; $C_2H_5OH:H_2O:N_2 = 0.5:1.5:98$; $Q_{Tot} = 1000\,(sp)cm^3/min$; GHSV: $15{,}000\,h^{-1}$.

Catalyst	S_{CH_4} (%)	S_{CO} (%)	S_{CO_2} (%)	S_{H_2} (%)	$S_{C_2H_4}$ (%)	$S_{C_3H_6O}$ (%)	S_C (%)
1-Pt/Al_2O_3	39	45	4	23	9	–	–
1-Pt/CeO_2	32	21	26	29	–	16	–

Ethanol conversion was lower than 20% on both supports, but only traces of hydrogen were found with CeO_2, while the formation of ethyl ether and hydrogen was observed with Al_2O_3. Alumina is known to be active in dehydration reactions, and ethylene [35] and ethyl ether can form in parallel during catalytic dehydration of ethanol, with a relative selectivity depending on the experimental conditions [36].

In Fig. 4 the comparison of catalytic activity in ESR reaction is reported for the 1-Pt/Al_2O_3 and 1-Pt/CeO_2 samples in terms of ethanol conversion and hydrogen yield as a function of time on stream.

Experimental results show that total ethanol conversion is reached for both, but the hydrogen yield is higher and more stable for 1-Pt/CeO_2 catalyst. In particular, the ceria supported catalyst shows an initial H_2 yield about 20% higher than that shown by the alumina supported sample, and this difference increases to about 30% after 180 min.

Moreover, the average deactivation rate in the case of alumina supported sample is about five times higher than that of the ceria supported sample (−0.0140%/min versus −0.0028%/min).

Also the products distribution was strongly influenced by the support nature, as reported in Fig. 5. For a better comparison, the selectivity values to the main reaction products after 3 h of time on stream are shown in Table 3. While 1-Pt/Al_2O_3 catalyst is highly selective to CO, and CH_4, a very different product distribution is obtained for 1-Pt/CeO_2 catalyst, with a much higher selectivity to H_2 and CO_2, and a lower CO selectivity.

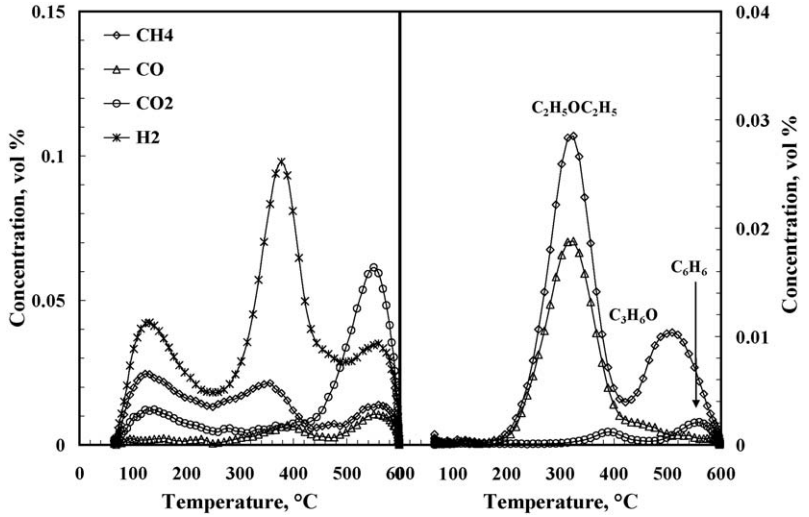

Fig. 6. TPD spectra of reaction products adsorbed over Al_2O_3 after 3 h of time on stream of ethanol steam reforming reaction at 300 °C with stoichiometric water to ethanol molar ratio.

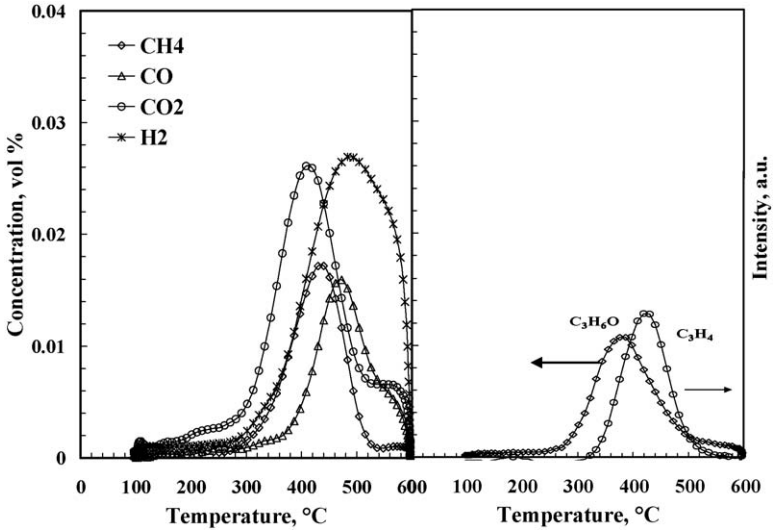

Fig. 7. TPD spectra of reaction products adsorbed over CeO_2 after 3 h of time on stream of ethanol steam reforming reaction at 300 °C with stoichiometric water to ethanol molar ratio.

3.4. Temperature programmed desorption

The TPD profiles collected after ethanol SR test at 300 °C with Al_2O_3 and CeO_2 are shown in Figs. 6 and 7, respectively. Hydrogen was the main desorption product from Al_2O_3, being divided in three peaks (130, 377 and 559 °C). At 130 °C also the desorption of CH_4 and CO_2 was observed, likely related to ethanol decomposition and WGS reactions. At about 300 °C diethyl ether desorbed along with H_2, CH_4 and a small amount of CO. Diethyl ether can be obtained by the reaction between adsorbed acetaldehyde molecules [37], or by reaction of two ethanol molecules forming water [38]. At higher temperature (500–600 °C) the desorption of CO_2, C_3H_6O and C_6H_6 was detected. Acetone formation can be explained by the reaction of acetaldehyde with adsorbed methyl groups [37], or by reaction of two ethanol molecules adsorbed [39].

CH_4, CO, CO_2 and H_2 desorbed from CeO_2 in the range 200–600 °C, their peaks being centered at 440, 472, 408 and 493 °C, respectively. The desorption of acetone and very small amount of propadiene was also observed; acetone desorbed at higher temperature compared with Al_2O_3.

The TPD spectra of reaction products from 1-Pt/Al_2O_3 and 1-Pt/CeO_2 after 3 h of time on stream are reported in Figs. 8 and 9, respectively.

For 1-Pt/Al_2O_3 at low temperatures (200–300 °C) the desorption of adsorbed ethanol was detected, its cracking producing CH_4, CO and H_2. Diethyl ether desorbed with a maximum at 268 °C, the intensity of the peak being lower if compared with Al_2O_3. At increasing temperature TPD spectra were dominated by the desorption of H_2 and CO, whose spectra can be divided into two contributions, the first centered at about 425 °C and the second at 510 °C. CO_2 and acetone were also desorbed with a peak temperature of about 450 °C. In the temperature range 300–600 °C the desorption of benzene was observed.

TPD spectra obtained for 1-Pt/CeO_2 after ethanol SR test were different with respect to 1-Pt/Al_2O_3. While in the low temperature range (200–300 °C) there was only a small desorption of H_2, it became strongly larger in the range from 300 to 600 °C, with two contributions centered at 410 and 560 °C. CO_2 was desorbed at a peak temperature of 340 °C and the desorption continued until to 600 °C. CO was desorbed with two contributions at peak temperatures of 425 and 570 °C. The desorption of a small amount

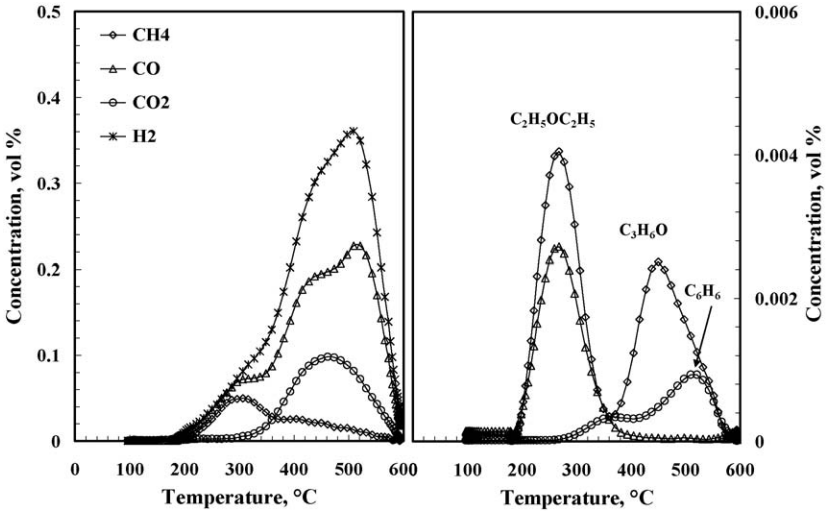

Fig. 8. TPD spectra of reaction products adsorbed over 1-Pt/Al_2O_3 after 3 h of time on stream of ethanol steam reforming reaction at 300 °C with stoichiometric water to ethanol molar ratio.

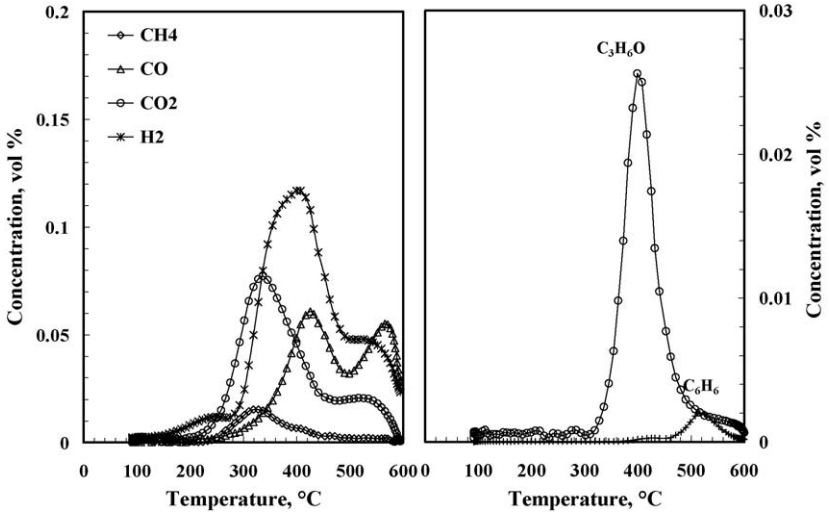

Fig. 9. TPD spectra of reaction products adsorbed over 1-Pt/CeO_2 after 3 h of time on stream of ethanol steam reforming reaction at 300 °C with stoichiometric water to ethanol molar ratio.

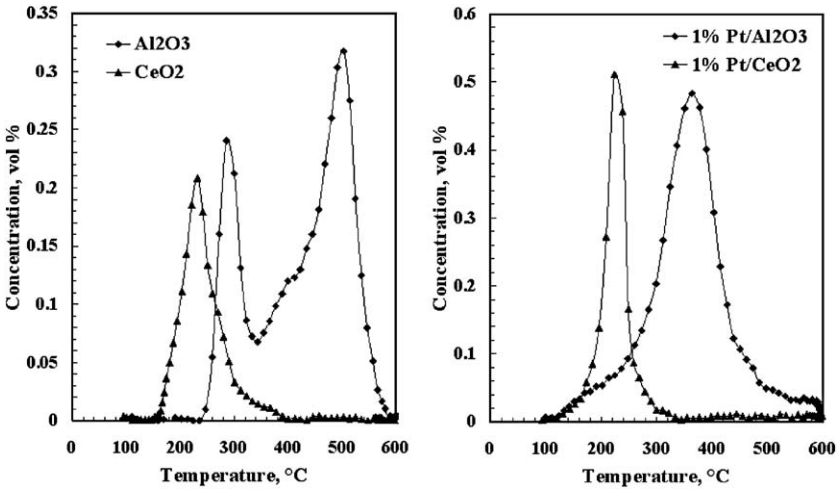

Fig. 10. TPO of carbon deposited on supports and Pt catalysts after 3 h of time on stream of ethanol steam reforming at 300 °C with stoichiometric water to ethanol molar ratio.

of CH_4 was also observed at about 300 °C, while acetone desorbed at 400 °C and benzene formation was clearly evidenced at 520 °C.

The amount of products desorbed from Al_2O_3 surface is higher than that from CeO_2. Upon platinum loading, the amount of desorption products increased, due to the higher activity of the catalyst with respect to the support. On both supports and catalysts the main desorption product is hydrogen, its formation starting at lower temperature (100–200 °C) on Al_2O_3 and Pt/Al_2O_3 catalysts. The source of hydrogen is the dehydrogenation of molecularly adsorbed ethanol, at least up to 200 °C. Ethanol was found to adsorb on various metal oxide surfaces by the dissociation of the OH bond, with the proton going to a surface lattice oxygen and the ethoxide species bonded to the surface cation. Adsorbed ethoxide species were detected upon the adsorption of ethanol on various oxide surface including TiO_2 [40], CeO_2 [41,21] and Al_2O_3 [42]. Above 200 °C, no molecularly adsorbed ethanol was detected, and the production of H_2, found at high temperature for all catalysts could be assigned to the desorption of H_2 previously formed during the different steps of ethanol dehydrogenation. Taking into account that on Pt/Al_2O_3 catalyst H_2 selectivity decreases in the course of reaction we can state that the metal surface (the active surface site for the dehydrogenation of ethanol) is poisoned and, consequently, the efficiency of the support comes to the forefront. Erdöhelyi et al. [50] have reported the formation of acetate species at 300 °C on Al_2O_3 supported catalyst. They stated that these species are located primarily on the support and can poison the reaction, and assume that they can hinder the migration of ethoxide to the metal, causing the decrease of hydrogen formation on metal sites. The desorption of CO_2 and H_2 at high temperature could be attributed to the acetate decomposition on Al_2O_3 surface. In the same work they suggest that acetate species formed on the supporting oxide migrate to the vicinity of the metal at high temperature and decompose there. Cordi and Falconer [43] found by TPD experiments that acetic acid adsorbed on Al_2O_3 decomposes only above 300 °C and the reaction was not complete at 600 °C; CO, CO_2, CH_4 and H_2 were found as decomposition products. They supposed that the carbon–carbon bond was cleft to form CO and CO_2 from α carbon and some of the resulting CH_3 groups were hydrogenated to CH_4. The amount of CH_4 was much smaller than that of CO + CO_2, the rest of the β carbon, however, remained on the surface.

Over metal oxides both dehydrogenation to acetaldehyde and dehydration to ethylene occur, depending on the nature of the oxides. The dimerization of aldehydes is also possible through aldolization reaction. From two acetaldehyde molecules crotonaldehyde formation also occurs through dehydration [50]. Based on TPD results we can state that

(i) Al_2O_3 mainly favors ethanol dehydration reactions to ethyl ether and/or ethylene.
(ii) Platinum addition favors the dehydration to ethylene.
(iii) In the case of ceria, acetone is the main secondary product, likely formed by acetate species; the deactivation may be due to the limited dehydrogenation of the CH_x formed after the acetate decomposition.
(iv) The presence of platinum favored the desorption of acetone from CeO_2 surface, since the formation of acetone during ethanol steam reforming reaction was observed over 1-Pt/CeO_2, while was not observed over CeO_2.

One of the Pt roles seems to be active in the hydrogenation reaction of coke precursors, with methane formation, as indicated by the increase of stability and CH_4 selectivity with Pt load.

Benzene desorbed from the surface of both catalysts. Benzene is a coke precursor, being intermediate in reactions such as aromatization, cyclization, polycondensation involved in coke formation, the main cause of catalyst deactivation. It is worthwhile to notice that benzene was desorbed from the Al_2O_3 surface, while no formation of benzene was observed with CeO_2. This should be related to the higher tendency to deactivation of Al_2O_3 with respect to CeO_2.

3.5. Temperature programmed oxidation

TPO profiles of supports and catalysts after ethanol steam reforming at 300 °C and TPD tests were obtained to investigate the presence of carbon deposits on their surface. They are shown in Fig. 10. CeO_2 shows one oxidation peak at 230 °C (shoulder at 280 °C), while for Al_2O_3 two oxidation peaks were observed, at 285 and 502 °C (shoulder at 400 °C). The TPO profile of 1-Pt/CeO_2 shows one peak at 223 °C, while 1-Pt/Al_2O_3 has different TPO profiles compared with Al_2O_3: one wide peak was observed at lower temperature (363 °C).

The lowering of the peak temperature in the catalyst could be related to the presence of noble metal, which favors the coke oxidation. No formation of CO was observed during TPO experiments. The coke content in used catalysts and supports is reported in Table 4. Compared with bare supports, the amount of coke deposited on platinum catalysts is higher, and does not show any significant higher reactivity at low temperature. The comparison between the Al_2O_3 and CeO_2, with and without Pt addition,

Table 4
Coke content of supports and catalysts used in ethanol steam reforming.

Samples	C (μmol/g_{cat})
Al_2O_3	138
CeO_2	70
1-Pt/Al_2O_3	232
1-Pt/CeO_2	116

shows that the carbon deposited on CeO_2 and 1-Pt/CeO_2 is lower than that deposited on Al_2O_3 and Pt/Al_2O_3.

The nature of the coke always is complex and its reactivity changes as a consequence of the formation mechanism. The more reactive coke, associated to the low temperature (~200 °C) CO_2 peak, may be derived from the first decomposition of products with a lower molecular weight, while the components of high temperature (>350 °C) coke consist of secondary reaction products or intermediates, such as polyaromatics, and result from hydrogen transfer and dehydrogenation reactions [44–46]. Carbon deposited on CeO_2 and Pt/CeO_2 surface was in lower amounts and, more important, it was more reactive than the carbon species deposited on Al_2O_3 and Pt/Al_2O_3 surface, confirming the beneficial role of the ceria support in the control of the coke precursors formation. The activity of coke formation is further improved with the Pt addition, likely due to the promotion of the hydrogenation reaction of CH_x coke precursors. In the case of Al_2O_3 supported catalysts, the more stable carbonaceous species poisoned easier the active sites of the catalyst, causing the higher deactivation rate observed.

Therefore, these results clearly show that 1-Pt/Al_2O_3 catalyst exhibits poor performance than 1-Pt/CeO_2 catalyst in terms of CO selectivity, hydrogen yield and stability.

3.6. Effect of metal loading on catalytic activity of Pt/CeO_2 samples

Following the above conclusion we addressed our work to investigate the Pt/CeO_2 catalysts starting from evaluating the effect of Pt load on the catalysts properties. The results of ethanol conversion and H_2 yield are compared in Fig. 11 as a function of time on stream for two additional Pt-CeO_2 catalysts, with, respectively, 3 and 5 wt% of noble metal. It is worthwhile to note that the transient time observed in the ethanol conversion curve for the 1-Pt load sample decreases by increasing the Pt loading and becomes not appreciable for the highest metal content.

In addition, by increasing the metal content both H_2 and CO_2 selectivities are increased and the CO selectivity is lowered. In particular, for 3-Pt/CeO_2 very low amounts of CO was noticed, that become undetectable for the 5-Pt/CeO_2 (Table 5) after 10 h of TOS.

Table 5
Selectivity to CH_4, CO, CO_2 and H_2 after 10 h of time on stream of 5-Pt/CeO_2 catalyst. Experimental conditions as in Table 3.

Catalyst	S_{CH_4} (%)	S_{CO} (%)	S_{CO_2} (%)	S_{H_2} (%)	$S_{C_2H_4}$ (%)	$S_{C_3H_6O}$ (%)	S_C (%)
5-Pt/CeO_2	40	0	60	37	–	–	–

The selectivities to H_2, CO and CO_2 are related via the water gas shift reaction, while the selectivity toward CH_4 is independent of that and is related only to the ethanol decomposition and steam reforming reactions. Therefore, the differences reaction products distribution indicate that the catalytic systems investigated have a different WGS activity, Pt/CeO_2 being much more active than Pt/Al_2O_3. The activity in WGS reaction is enhanced by increasing the metal loading.

Therefore, while under the reaction conditions investigated Pt/Al_2O_3 catalysts give poor performance in ethanol SR, Pt/CeO_2 catalysts are active and selective, full ethanol conversion being achieved already for 1 wt% Pt loading. On 5-Pt/CeO_2 the reaction products are exclusively CH_4, CO_2 and H_2. This indicates that on this catalyst, along with ethanol steam reforming, the decomposition of ethanol is also favored and the unconverted water favors the WGS reaction.

The simultaneous deactivation of the 1-Pt/CeO_2 catalyst and the acetone formation may be explained considering the presence of acetate species that accumulate during the low temperature ESR, hindering the formation of desirable ethoxide species, which are more mobile and migrate and subsequently dehydrogenate at the metal–support interface [47]. In this mild reaction conditions these acetate species are quite stable and may partially react to form acetone [48]. It has been suggested that during acetic acid reforming on supported Pt, acetone and acetic acid are responsible for the catalyst deactivation due to the blockage of active sites, probably the metal-support interfaces, by oligomers formation [49].

Anyway, even if in competition with the ethanol reaction for hydrogen formation, the consequences of the acetone formation on the catalyst stability are not so dramatic if compared with the hydrogen yield decrease observed in the case of Pt/Al_2O_3 catalyst.

The higher deactivation rate observed for the Al_2O_3 supported catalyst suggests that during the reaction the catalyst surface changes and, as a consequence of this process, Pt sites are poisoned

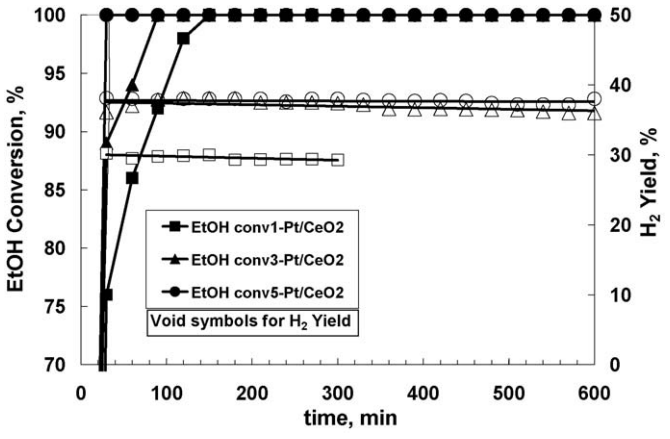

Fig. 11. Effect of Pt load on ethanol conversion and H_2 yield versus time on stream for Pt/CeO_2 catalysts. *Experimental conditions*: T = 300 °C; C_2H_5OH = 0.5 vol%; $C_2H_5OH:H_2O:N_2$ = 0.5:1.5:98; Q_{Tot} = 1000 (stp)cm^3/min; GHSV: 15,000 h^{-1}.

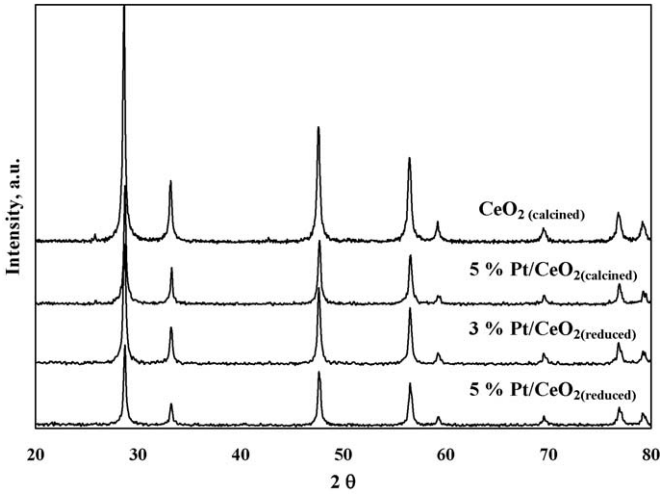

Fig. 12. XRD patterns of Pt/CeO_2 catalysts before and after reduction treatment.

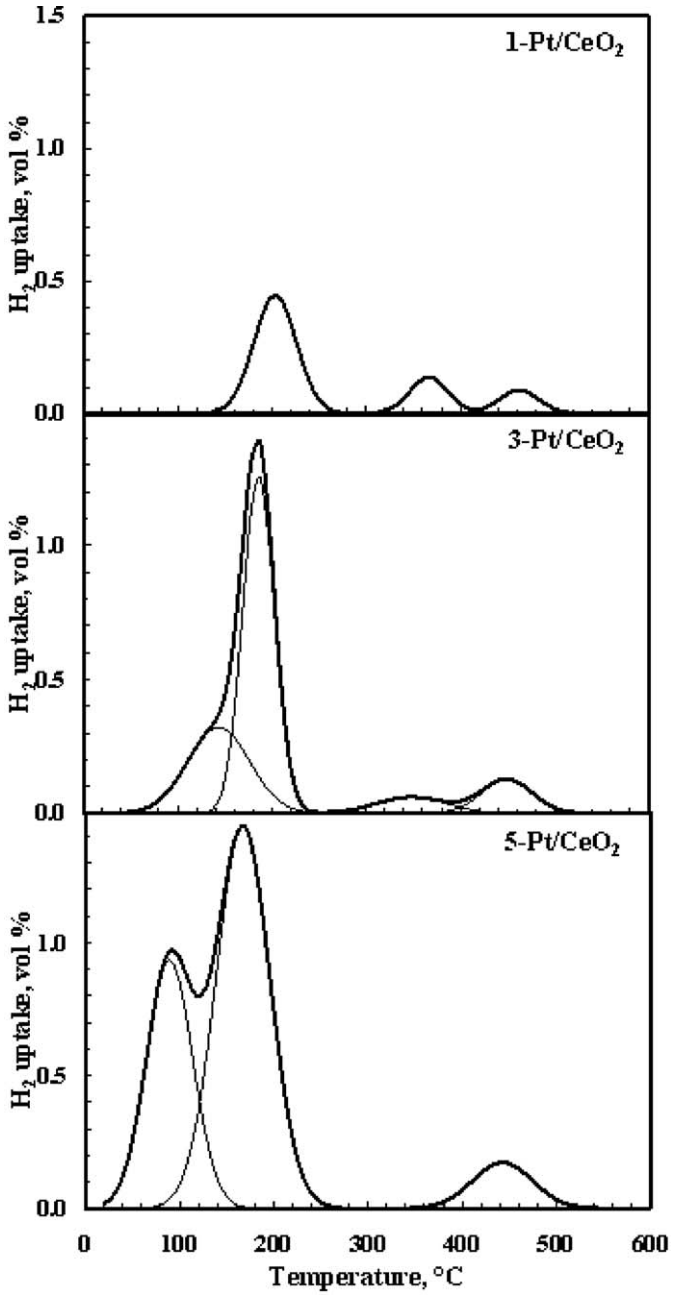

Fig. 13. TPR profiles of Pt/CeO_2 catalysts.

and the efficiency of the support comes to the forefront. It is possible that (i) Pt is oxidized during the reaction, and (ii) a surface species is formed which hinders the migration to the metal of ethoxide formed from ethanol decomposition, causing the decrease of hydrogen formation on the metal sites [50]. A comparison between ceria and alumina as supports suggests that secondary products formed on alumina poison platinum sites, likely due to the higher sites acidity that promote the dehydration of ethanol to ethylene [35], and to the lower ability to release/store oxygen with respect to ceria, that, in addition, is more able to promote the dissociation of molecules of the ROH type (e.g., H_2O and ethanol) [51].

XRD diffraction patterns of Pt/CeO_2 samples after hydrogen reduction are shown in Fig. 12. For comparison, the diffraction pattern relevant to the just calcined support and the 5-Pt/CeO_2 sample are also reported. For all spectra only CeO_2 signals

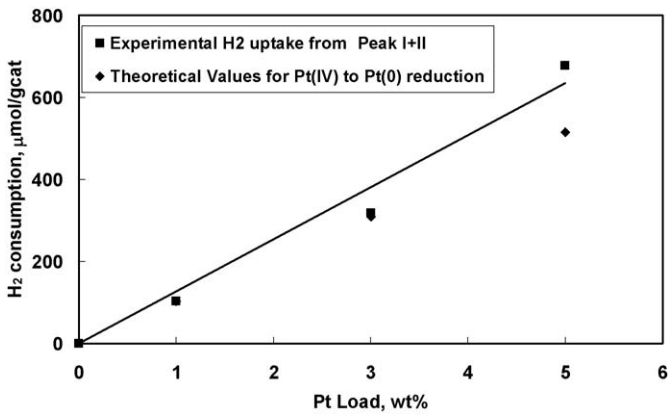

Fig. 14. H_2 consumption as a function of the Pt load for Pt/CeO_2 catalysts in the temperature range from RT to 300 °C and theoretical H_2 required for the Pt(IV) to Pt(0) reduction reaction.

corresponding to a fluorite-like structure ($2\theta = 28.5$, 33.3, 47.5, 56.4) were present, without any signal characteristic from platinum, likely due to high metal dispersion on the support.

In Fig. 13 is reported the TPR profile for the three Pt/CeO_2 catalysts, respectively, with 1, 3, and 5 wt% Pt nominal load. Results showed that in the higher temperature range ($T > 300$ °C) two peaks at 366 and 462 °C are observed for 1-Pt/CeO_2. By increasing the platinum content the intensity of the first peak decreases while that of the second increases. At the highest Pt loading (5 wt %) the two peaks are merged in a single one centered at 448 °C. Anyway, the effect of Pt is more evident for temperature lower than 300 °C, where the reduction profile changes considerably by increasing the Pt load. In particular, the profile of 1-Pt/CeO_2 exhibits a single symmetric reduction peak centered at 203 °C, indicating the high dispersion of PtO_x particles with uniform particle size distribution. By increasing the metal loading to 3 and 5 wt% the peak area increases and the peak temperature shifts to a lower value, while on 5-Pt/CeO_2 a new peak centered at 90 °C appears. A similar peak is present as a shoulder in the TPR profile of 3-Pt/CeO_2.

Therefore, we can say that for temperature lower than 300 °C the higher temperature reduction peak can be assigned to the presence on CeO_2 surface of highly dispersed PtO_x species and the presence of direct Pt–O–Ce bonding, where the strong interaction of PtO_x with the CeO_2 support retards the reduction of the supported PtO_x phase to metallic Pt [34].

By increasing the Pt load, the effectiveness of the PtO_x phase dispersion decreases, and the lower extent of the Pt–O–Ce bonding

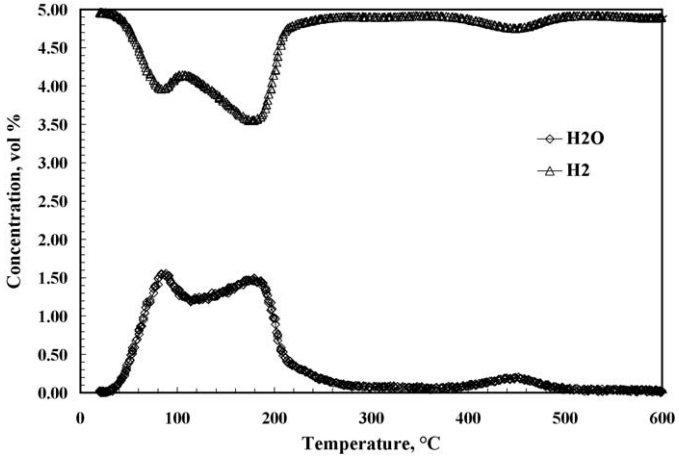

Fig. 15. H_2 consumption and H_2O formation during the TPR of 5-Pt/CeO_2 catalyst.

results in a lower reduction temperature, with the formation of metallic Pt at temperature lower than 90 °C. The temperature shift of the second reduction peak can be explained by considering the H_2 spillover from the metallic Pt previously formed [34,52].

The partial amounts of hydrogen uptake, calculated by integrating the peak areas after deconvolution, are reported in Fig. 14 as a function of nominal Pt load. It is observed that for all the three Pt/CeO_2 catalysts, if one consider the two peaks in the temperature range from RT to 300 °C, the hydrogen consumption is in good agreement with the amount calculated on the base of nominal Pt load, considering the 100% of the stoichiometric $Pt^{4+} \rightarrow Pt^0$ reaction, indicating that during the calcination step the CeO_2 support, at variance of Al_2O_3, stabilize the Platinum in the highest oxidation state. In Fig. 15 the hydrogen concentration profile and the water production are reported as a function of temperature during the H_2 TPR test of the 5-Pt/CeO_2 catalyst. The qualitative agreement is very good, and also the H_2 mass balance is verified, with the exception of the low temperature reduction peak. In particular, for the first reduction peak, centered at about 90 °C, we evaluate a H_2 uptake of 212 $\mu mol/g_{cat}$, versus a H_2O production of 413 $\mu mol/g_{cat}$. This apparent discrepancy can be explained by considering the presence of isolated hydroxyl groups on the CeO_2 surface, OH(I) sites, that can be reduced by H_2 spillover from the just formed metallic Pt particles [34,52].

4. Conclusions

We found that the CeO_2 supported 1 wt% Pt catalyst is more active, selective and stable than 1 wt% Pt on Al_2O_3 in the range 300–450 °C. With reference to catalyst deactivation we suggest that under the reaction conditions investigated Al_2O_3 is not able to promote the desorption of the secondary reaction products. As a consequence, its surface is poisoned and the ethanol decomposition process is hindered, leading to a marked decay in H_2 and CO_2 selectivity. Coke formation, investigated by TPO experiments, occurred on supports and catalysts. However, more stable carbonaceous species were found on Al_2O_3 and Pt/Al_2O_3 catalyst, likely responsible for the higher deactivation rate with respect to CeO_2 supported Pt catalyst.

The characterizations of catalysts reveal the presence of very well dispersed PtO_x, stabilized in the highest oxidation state by ceria during the calcination step, in contrast with Al_2O_3.

Ethanol decomposition to CH_4, CO and H_2, ethanol dehydrogenation to acetaldehyde, acetate formation following acetone production, were the primary reactions occurring at low temperature.

The characterization of the spent catalysts by TPD has confirmed that ethanol dehydration to ethylene was the main reaction over Al_2O_3, further favored in the presence of platinum. With CeO_2 surface acetone formation was observed, but in this case platinum favored acetone desorption from the catalyst surface. Desorption and conversion of secondary products, due to the greater ability of CeO_2 to release/store oxygen also resulted in higher stability with respect to alumina supported catalysts.

Increasing Pt loading to 5 wt % the intermediate reaction products such as acetaldehyde and acetone were completely converted into hydrogen, carbon dioxide and methane, and the produced CO was converted to CO_2 through WGS reaction. Therefore, CO was practically absent in the reformate. This result is very important with respect to the limited CO concentrations required for feeding PEM fuel cells.

References

[1] J.R. Rostrup-Nielsen, in: J.R. Anderson, M. Boudart (Eds.), Catalysis Science and Technology, vol. 5, Springer, Berlin, 1984, p. 1.
[2] G.W. Huber, J.W. Shabaker, J.A. Dumesic, Science 300 (2003) 2075.
[3] R.D. Cortright, R.R. Davda, J.A. Dumesic, Nature 418 (2002) 964.
[4] G.A. Deluga, J.R. Salge, L.D. Schmidt, X.E. Verykios, Science 303 (2004) 993.
[5] E.Y. Garcia, M.A. Laborde, Int. J. Hydrogen Energy 16 (1991) 307.
[6] K. Vasudeva, N. Mitra, P. Umasankar, S.C. Dhingra, Int. J. Hydrogen Energy 21 (1996) 13.
[7] I. Fishtik, A. Alexander, R. Datta, D. Geana, Int. J. Hydrogen Energy 25 (2000) 31.
[8] V. Mas, R. Kipreos, N. Amadeo, M. Laborde, Int. J. Hydrogen Energy 31 (2006) 21.
[9] A. Haryanto, S. Ferno, N. Murali, S. Adhikari, Energy Fuels 19 (2005) 2098.
[10] M.C. Sánchez-Sánchez, R.M. Navarro, J.L.G. Fierro, Int. J. Hydrogen Energy 32 (2007) 1462.
[11] N. Homs, J. Llorca, P. Ramírez de la Piscina, Catal. Today 116 (2006) 361.
[12] A.N. Fatsikostas, D.I. Kondarides, X.E. Verykios, Catal. Today 75 (2002) 145.
[13] S. Freni, S. Cavallaro, N. Mondello, L. Spadaro, F. Frusteri, J. Power Sources 108 (2002) 53.
[14] F. Haga, T. Nakajima, H.B. Miya, S. Mishima, Catal. Lett. 48 (1997) 223.
[15] J. Llorca, N. Homs, J. Sales, P. Ramìrez de la Piscina, J. Catal. 209 (2002) 306.
[16] J.P. Breen, R. Burch, H.M. Coleman, Appl. Catal. B: Environ. 39 (2002) 65.
[17] D.K. Liguras, D.I. Kondarides, X.E. Verykios, Appl. Catal. B: Environ. 43 (2003) 345.
[18] V. Fierro, O. Akdim, C. Mirodatos, Green Chem. 5 (2003) 20.
[19] J.H. Sinfelt, Adv. Catal. 23 (1973) 91.
[20] D.C. Grenoble, M.M. Estat, D.F. Ollis, J. Catal. 67 (1981) 90.
[21] A. Yee, S.J. Morrison, H. Idriss, J. Catal. 191 (2000) 30.
[22] T. Bunluesin, R.J. Gorte, G.W. Graham, Appl. Catal. B: Environ. 15 (1988) 107.
[23] A. Trovarelli, Catal. Rev. Sci. Eng. 38 (1996) 439.
[24] J. van Doorn, J. Varloud, P. Meriaudeau, V. Peric?n, M. Chevrier, C. Gauthier, Appl. Catal. B: Environ. 1 (1992) 117.
[25] Y. Chen, Z. Shao, N. Xu, Energy Fuels 22 (2008) 1873.
[26] S.M. de Lima, A.M. Silva, U.M. Graham, G. Jacobs, B.H. Davis, L.V. Mattos, F.B. Noronha, Appl. Catal. A: Gen. 352 (2009) 95.
[27] S.M. de Lima, A.M. Silva, I.O. da Cruz, G. Jacobs, B.H. Davis, L.V. Mattos, F.B. Noronha, Catal. Today 138 (2008) 162.
[28] S.M. de Lima, A.M. Silva, I.O. da Cruz, G. Jacobs, B.H. Davis, L.V. Mattos, F.B. Noronha, J. Catal. 257 (2008) 356.
[29] P. Ciambelli, V. Palma, A. Ruggiero, Appl. Catal. B: Environ. 96 (2010) 190.
[30] C. Hwang, C. Yeh, J. Mol. Catal. A: Chem. 112 (1996) 295.
[31] H. Lieske, G. Lietz, H. Spindler, J. Völter, J. Catal. 81 (1983) 8.
[32] H.C. Yao, Y.F. Yu Yao, J. Catal. 86 (1984) 254.
[33] C. de Leitenburg, A. Trovarelli, J. Kašpar, J. Catal. 166 (1997) 98.
[34] W. Lin, A.A. Herzing, C.J. Kiely, I.E. Wachs, J. Phys. Chem. C 112 (2008) 5942.
[35] A.N. Fatsikostas, X.E. Verykios, J. Catal. 225 (2004) 439.
[36] G. Chen, S. Li, F. Jiao, Q. Yuan, Catal. Today 125 (2007) 111.
[37] H. Idriss, C. Diagne, J.P. Hindermann, A. Kiennemann, M.A. Barteau, J. Catal. 155 (1995) 219.
[38] F. Mariño, M. Boveri, G. Baronetti, M. Laborde, Int. J. Hydrogen Energy 26 (2001) 665.
[39] B. Zhang, X. Tang, Y. Li, W. Cai, Y. Xu, W. Shen, Catal. Commun. 7 (2006) 367.
[40] J. Raskó, A. Hancz, A. Erdohelyi, Appl. Catal. A: Gen. 269 (2004) 13.
[41] A. Yee, S.J. Morrison, H. Idriss, J. Catal. 186 (1999) 279.
[42] S. Golay, R. Doepper, A. Renken, Appl. Catal. A: Gen. 172 (1998) 97.
[43] E.M. Cordi, J.L. Falconer, J. Catal. 162 (1996) 104.
[44] M. Guisnet, P. Magnoux, Appl. Catal. A: Gen. 212 (2001) 83.
[45] M.R. Jovanovic, P.S. Putanov, Appl. Catal. A: Gen. 159 (1997) 1.
[46] J. Barbier, P. Marecot, N. Martin, A. Elassal, R. Maurel, Stud. Surf. Sci. 40 (1980) 53.
[47] A. Platon, H.S. Roh, D.L. King, Y. Wang, Top. Catal. 46 (2007) 374.
[48] M. Fleisher, V. Stonkus, I. Liepina, K. Edolfa, D. Jansone, L. Leite, E. Lukevics, Presented at *ECSOC-13*, Section G: Computational Chemistry, published online: 30 October 2009.
[49] K. Takanabe, K. Aika, K. Seshan, L. Lefferts, J. Catal. 227 (2004) 101.
[50] A. Erdöhelyi, J. Raskò, T. Kecskés, M. Tòth, M. Dömök, K. Baàn, Catal. Today 116 (2006) 367.
[51] G. Jacobs, R.A. Keogh, B.H. Davis, J. Catal. 245 (2007) 326.
[52] R.W. McCabe, C. Wong, H.S. Woo, J. Catal. 114 (1988) 354.